

Absolute colors and phase coefficients of trans-Neptunian objects: $H_V - H_R$ and relative phase coefficients

C. Ayala-Loera,^{1*} A. Alvarez-Candal,¹ J. L. Ortiz,² R. Duffard,²
E. Fernández-Valenzuela,^{2,3} P. Santos-Sanz,² and N. Morales,²

¹Observatório Nacional / MCTIC, Rua General José Cristino 77, Rio de Janeiro, RJ, 20921-400, Brazil.

²Instituto de Astrofísica de Andalucía, CSIC, Apt 3004, 18080, Granada, Spain.

³Florida Space Institute (FSI) at University of Central Florida, 02354 Research Parkway, Suite 284, Orlando, FL, 32826, USA.

Accepted XXX. Received YYY; in original form ZZZ

ABSTRACT

The trans-Neptunian objects (TNOs) are small Solar System bodies at large distances from the Sun. As such, their physical properties are difficult to measure. Accurate determination of their physical parameters is essential to model and theorize the actual composition and distribution of the population, and to improve our understanding of the formation and evolution of the Solar System. The objective of this work is to construct phase curves in two filters, V and R , of a large TNO sample obtaining absolute magnitudes (H) and phase coefficients (β), and study possible relations between them and other physical parameters (orbital elements, sizes, and albedos). We used our own data, together with data from the literature, to create the phase curves assuming an overall linear trend. We obtained new magnitudes for 35 TNOs, 27 in the V filter and 35 in the R filter. These magnitudes, together with data from the literature, allowed us to obtain absolute magnitudes, 114 in the V filter and 113 in the R filter, of which 106 have both. From the search for correlations we found a strong anticorrelation between $H_V - H_R$ and $\Delta\beta = \beta_V - \beta_R$, which is probably more related to surface structure than to composition or size of the objects.

Key words: Kuiper belt objects: general – methods: observational – technique: photometric

1 INTRODUCTION

The trans-Neptunian objects, TNOs, are distant objects left-overs of the protoplanetary disk where the planets formed. The understanding of their physical properties sets important constraints to improve the evolution models of the Solar System (Mueller et al. 2010).

Nowadays, the Minor Planet Center¹ lists around 2,300 TNOs. Unfortunately, just a few hundreds of them have high-quality physical studies, due to their orbital and size distributions, that produce few objects brighter than $V_{mag} \sim 17$. Among the techniques used to study TNOs, photometry is the less expensive one (in terms of observing time). Photometric studies allow to obtain information of a good number of TNOs via apparent magnitudes and colors. The first are measurements of the integral reflected light by the TNO surface, subjected to the geometry of the observation and physical properties, such as diameter (D)

and albedo (p), while the latter is a measure of the slope of the spectral reflectance of the object. Apparent magnitudes can be used to obtain absolute magnitudes (H) if the observational circumstances are known. The absolute magnitude is the mean apparent magnitude, over a rotation cycle of the object, observed at zero phase angle, and both at 1 AU from the Sun and the Earth. In practice, H should be computed using phase curves and the formalism of Muinonen et al. (2010). A phase curve shows the change of the apparent magnitude, normalized to unit distance from the Earth and the Sun, with the phase angle (α). Nonetheless, due to the large distances where the TNOs reside, α (the arc that subtends the distance Sun-Earth as seen from the object) can only reach values as large as $\sim 3^\circ$, while the centaurs (representatives of the TNO population orbiting closer to the Sun) can be observed up to phase angles $\sim 7^\circ$. In these small ranges the phase curves can be approximated by a linear function (see, for instance, Alvarez-Candal et al. 2016) with due caution for possible opposition surges at phase angles close to zero.

* E-mail: madelcarmen@on.br

¹ <http://www.minorplanetcenter.net/iau/mpc.html>

The absolute magnitude is of interest because it can be

used as a proxy for size through

$$D [km] = C \times 10^{-H/5} p^{-1/2}, \quad (1)$$

where C is a constant.

On the other hand, colors are the difference of two magnitudes measured using two filters with different effective wavelengths, λ_1 and λ_2 , and, as mentioned, are related to the reflectance spectrum of the objects, or, in other words, to their surface composition. However, even if different colors might imply different compositions, they cannot be used to infer it, but just as a first approach (Doressoundiram et al. 2008; Barucci et al. 2011).

The TNOs show a great diversity of colors, ranging from neutral to very red (Barucci et al. 2005). It has been suggested that colors of TNOs together with other properties, such as sizes and albedos at different wavelengths, are used to help describe their surfaces properties and evolution (Luu & Jewitt 1996; Pike, et al. 2017). However, laboratory work of Kaňuchová, et al. (2012) showed that fully weathered organic materials variate refractive properties of the materials and turn back in the color–color diagrams, such as a result suggest that colors themselves might not be entirely useful to explain the TNOs evolution. Thus, the color diversity of TNOs must be explained taking in account nurture and nature scenarios.

For instance, Peixinho et al. (2012) reported a bimodal ($B - R$) distribution of centaurs and small TNOs with a gap in ($B - R$) ~ 1.6 . Such a bimodality was independent of their orbital distribution and could be explained by different location of origin and/or disruptive collisions processes. Also, Lacerda et al. (2014) reported two groups of mid-sized TNOs based in albedo and color: one bright and red, while the other is dark and neutral, with no dynamical segregation. Such a color-albedo separation was explained as different birth locations and is considered as evidence of a break in the composition continuity of the protoplanetary disk.

In a previous work (Alvarez-Candal et al. 2016, hereafter paper 1) we analyzed the absolute magnitudes (H_V) and phase coefficients (β_V), of 110 TNOs in the V band. The methodology we used in paper 1 was slightly different than the presented here. We only used V magnitudes. In cases when only R magnitudes were available, we transformed them to V magnitudes using the weighed average ($V - R$) for the object. In the present work we extend our analysis by including data in the R band, i.e., H_R and β_R , and an updated list of magnitudes, some observed by ourselves and other from the literature not included before. With this, we aim at gaining a deeper comprehension on the surface characterization of TNOs. Of special interest is the “absolute color”, $H_V - H_R$, that is proportional to the ratio of albedos (Eq. 1) and does not have any phase-related effect, providing a zero-phase approximation to the reflectance spectrum. We also define the “relative phase coefficient” as $\Delta\beta = \beta_V - \beta_R$ and study its relationship with the absolute color and their relation with other typical parameters.

This paper is organized as follows: in the next section we described our new observations, in Sect. 3 we explain the method used, while in Sects. 4 and 5 we present and discuss our results.

2 OBSERVATIONS AND DATA REDUCTION

New observations of 35 objects are reported in this work. The observations were carried out using the 2.2-m telescope, at the Calar Alto Observatory (Spain), and the Southern Astrophysical Research (SOAR) Telescope, 4.1-m telescope, located at Cerro Tololo Inter-American Observatory (Chile). The observations were carried out using the V and R filters, with a total exposure time of 1800 s per filter, split, typically, into 3×600 s. No differential tracking was used since the sum of shorter exposures allows us to minimize trailing on the images, for example a typical centaur can move up to about 2 arcsecs in 10 minutes, therefore, using exposure times of 300 s the length of the trail is about the typical FWHM of the images. Also, short exposures help to reduce the effects of background sources, hot pixels, and cosmic rays hits. Standard stars from Landolt (1992) were also observed at different airmasses ($\lesssim 1.4$) to transform the instrumental magnitudes to the standard system.

All images were bias and flat-field corrected in the usual way using daily calibration files and standard IRAF routines². The images of the science objects were then aligned, using `imalign`, and median combined, using `imcombine`. The median combination is useful as it removes hot pixels and cosmic ray hits. We used the task `phot` to do aperture photometry of the science object and the standard stars, using a fixed aperture to obtain apparent instrumental magnitudes. In the few cases, crowded fields for example, where it was not possible to perform aperture photometry, we used aperture correction.

We followed the procedures outlined in paper 1 to correct the apparent instrumental magnitudes of atmospheric extinction, to compute the zero points of the nights (or used averages when necessary), and to propagate the corresponding errors. Finally, we calculated the reduced magnitudes,

$$M(1, 1, \alpha) = M - 5 \log(r\Delta), \quad (2)$$

where Δ is the topocentric distance of the object, and r is its heliocentric distance. Both were obtained from JPL-Horizons ephemeris³. All information is contained in Table 1.

3 METHODS

As we did in paper 1, we used our own data, complemented by data collected from the literature. All references are given in Table 4. References already provided in paper 1 are not repeated here.

In order to obtain H and β we fitted a 1st degree polynomial to the reduced magnitudes according to

$$M(1, 1, \alpha) = H + \alpha \times \beta. \quad (3)$$

The solutions to Eq. 3 are H , as the y-intercept, and β as the slope. Note that the same equation applies for V and R data.

² IRAF is distributed by the National Optical Astronomy Observatory, which is operated by the Association of Universities for Research in Astronomy (AURA) under a cooperative agreement with the National Science Foundation.

³ <http://ssd.jpl.nasa.gov/horizons.cgi>

Table 1. Observations

Object	V	R	Night	r (AU)	Δ (AU)	α ($^\circ$)	Telescope	Notes
19308 1996 TO ₆₆	20.91±0.249	20.17±0.176	2014-07-20	47.1403	46.9431	1.2159	CAHA	1
44594 1999 OX ₃	20.99±0.275	20.06±0.102	2014-07-20	19.9503	19.3693	2.4347	CAHA	1
47932 2000 GN ₁₇₁	21.00±0.103	20.71±0.080	2014-06-22	28.4215	27.6271	1.2949	SOAR	1
82158 2001 FP ₁₈₅	22.30±0.214	21.56±0.091	2014-07-20	35.7917	35.8120	1.6249	CAHA	1
82158 2001 FP ₁₈₅	...	22.15±0.531	2014-07-18	35.7902	35.7788	1.6260	CAHA	1
82155 2001 FZ ₁₇₃	21.55±0.147	20.95±0.112	2014-05-30	32.5456	31.7748	1.1679	SOAR	1
82155 2001 FZ ₁₇₃	21.74±0.170	21.70±0.182	2014-06-22	32.5507	32.0636	1.5808	SOAR	1
2001 KD ₇₇	22.25±0.149	21.35±0.118	2014-05-30	36.0591	35.1262	0.6455	SOAR	1
2001 QC ₂₉₈	23.36±0.687	23.14±0.635	2014-07-22	40.7801	40.1979	1.1823	CAHA	
275809 2001 QY ₂₉₇	22.31±0.167	21.59±0.128	2014-06-22	43.5248	42.9332	1.0962	SOAR	1
119951 2002 KX ₁₄	20.77±0.150	20.12±0.121	2014-05-30	39.2447	38.2325	0.0920	SOAR	1
119951 2002 KX ₁₄	20.71±0.095	20.18±0.068	2014-06-22	39.2422	38.2758	0.4645	SOAR	1
120178 2003 OP ₃₂	...	19.79±0.042	2014-07-20	41.9373	41.1515	0.8933	CAHA	1
307616 2003 QW ₉₀	21.09±0.324	20.99±0.143	2014-07-22	43.6784	43.3774	1.2798	CAHA	
120216 2004 EW ₉₅	21.23±0.118	22.08±0.372	2014-06-22	27.0915	26.4941	1.7573	SOAR	1
90568 2004 GV ₉	20.22±0.145	19.61±0.111	2014-05-30	39.3563	38.4608	0.6945	SOAR	1
2004 NT ₃₃	20.73±0.107	20.29±0.046	2014-07-20	38.6737	37.9280	1.0360	CAHA	1
307982 2004 PG ₁₁₅	21.20±0.365	20.58±0.152	2014-07-19	37.4889	36.6666	0.9276	CAHA	1
145452 2005 RN ₄₃	20.03±0.137	19.74±0.110	2014-07-20	40.6419	39.8866	0.9721	CAHA	1
145480 2005 TB ₁₉₀	21.18±0.247	20.71±0.139	2014-07-20	46.2178	45.5999	1.0111	CAHA	1
202421 2005 UQ ₅₁₃	21.71±0.404	20.43±0.198	2014-07-20	48.3909	48.2745	1.1980	CAHA	1
248835 2006 SX ₃₆₈	21.81±0.459	21.24±0.238	2014-07-20	12.9767	13.1433	4.3995	CAHA	1
278361 2007 JJ ₄₃	...	20.35±0.265	2014-07-17	41.2853	40.6122	1.0608	CAHA	1
2007 JK ₄₃	20.90±0.146	20.58±0.154	2014-07-22	23.6749	23.0767	2.0091	CAHA	
2007 OC ₁₀	21.14±0.166	20.62±0.163	2014-07-22	35.6835	34.8029	0.8284	CAHA	
2008 OG ₁₉	...	22.13±0.385	2014-07-18	38.5786	37.5909	0.3652	CAHA	1
2008 OG ₁₉	...	21.53±0.385	2014-07-17	38.5786	37.5939	0.3838	CAHA	1
2008 OG ₁₉	21.07±0.104	20.58±0.076	2014-06-22	38.5781	37.7704	0.9270	SOAR	1
2008 OG ₁₉	20.50±0.140	20.04±0.106	2014-05-30	38.5777	38.0398	1.2894	SOAR	1
65489 Ceto	...	20.84±0.188	2014-07-20	35.2266	34.9560	1.5970	CAHA	
65489 Ceto	22.06±0.354	22.56±0.646	2014-07-22	35.2314	34.9913	1.6089	CAHA	1
2060 Chiron	18.30±0.066	18.07±0.040	2014-07-19	17.8793	17.2129	2.5103	CAHA	1
2060 Chiron	...	17.88±0.048	2014-07-18	17.8786	17.2239	2.5426	CAHA	1
5145 Pholus	...	21.22±0.309	2014-07-22	25.8855	25.1171	1.4889	CAHA	
120347 Salacia	21.24±0.245	20.17±0.128	2014-07-19	44.4793	44.0186	1.1759	CAHA	1
174567 Varda	20.38±0.143	19.80±0.110	2014-05-30	47.2155	46.2716	0.4555	SOAR	1

(1) Average ext. coeff.

The linear fit, although simple, minimizes the number of free parameters and describes well enough the observational data, especially considering the restricted range of α we are using. While fitting, the reduced magnitude was weighted by its error, which is the same error that we have obtained from the apparent magnitudes.

As mentioned above, H represents a magnitude averaged over a rotation cycle. Unfortunately, many of the observations reported are snapshots at one unknown rotational phase. We will try to overcome this shortcoming following the procedure outlined below.

We generate 100,000 solutions of Eq. 3 by changing the reduced magnitude according to

$$M(1, 1, \alpha)_i = M(1, 1, \alpha) + rand_i \times \Delta m, \quad (4)$$

where Δm is the rotational light-curve amplitude (from [Thirouin et al. 2010, 2012](#); [Benecchi & Sheppard 2013](#)) and $rand_i$ is a random number extracted from a uniform distribution within the range $[-1, 1]$. In cases where Δm is unknown, we assumed $\Delta m = 0.14$, which is the median value of the distribution. Therefore, H and β will be the average over the 100,000 solutions of Eq. 4 and the errors their respective standard deviations.

Examples are shown in Fig. 1, where the panels in the left column show the observational data and the best fits. The right column shows the phase space covered by the 100,000 solutions, for data in both filters.

Most of the objects follow the expected behavior: brighter with decreasing phase angle, implying positive values of β . But, there are some objects that present a peculiar behavior, that is of a decrease of magnitude with decreasing phase angle, as seen in the middle and bottom panels of Fig. 1. Nevertheless, note that the phase space in these cases could allow solutions with positive values of β .

We obtained H_V for 114 objects and H_R for 113 objects, 105 objects have both. Figures for all our sample can be downloaded from http://extranet.on.br/alvarez/TN0s-Abs_Mags/phase-curves.tar.

3.1 Distributions

The distribution of the results, absolute magnitudes, phase coefficients, $H_V - H_R$, and $\Delta\beta$ obtained for our sample are

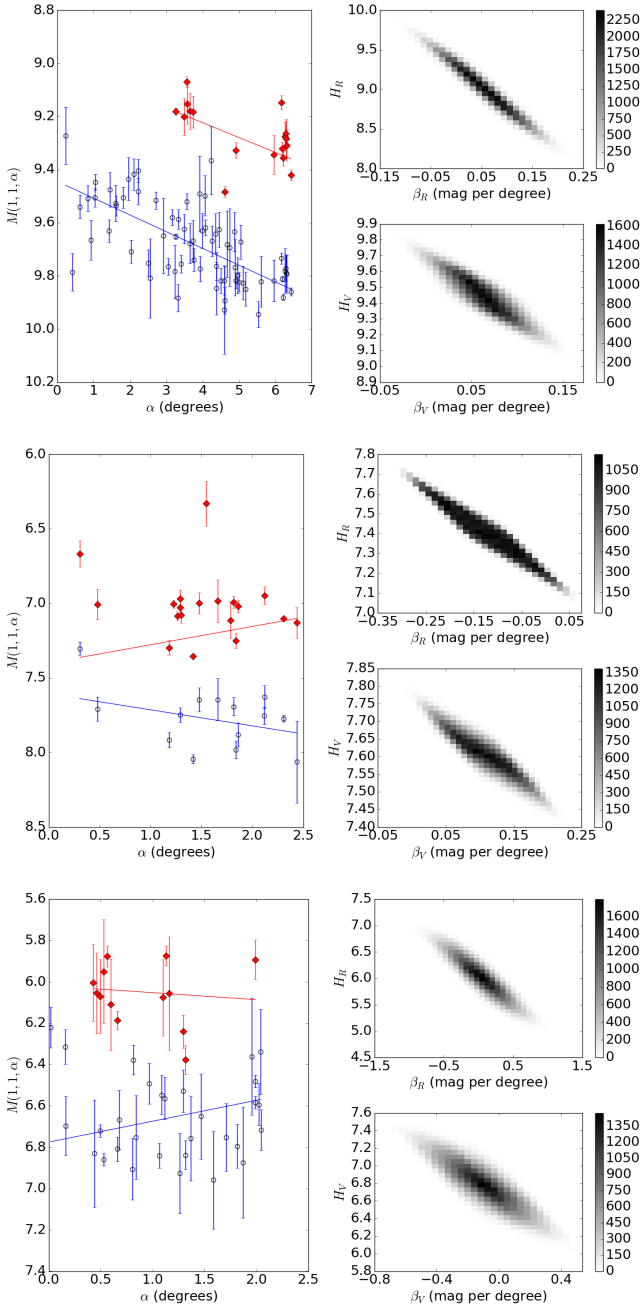


Figure 1. Phase curves of Thereus (top), 1999 OX₃ (middle) and 2000 GN₁₇₁ (bottom). The blue points correspond to $V(1, 1, \alpha)$, while the red diamonds indicate $R(1, 1, \alpha)$. The solid lines show our preferred solution to Eq.4. The density plots show the phase space covered by the 100,000 solutions (see text).

shown in Fig. 2. The minimum, average, and maximum of each distribution are reported in Table 2. At first glance, H_V (top left panel) and H_R (middle left panel) have similar overall distributions, with some differences in the detail. Likewise for β_V (top right) and β_R (middle right). In these last cases, most of the objects have positive values of the phase coefficient, with a clear maximum at about 0.02 mag per degree. Nonetheless, it is clear that negative values, even

Table 2. Notable values of the distributions

Quantity	<i>Min</i>	<i>Max</i>	<i>Mean</i>
H_V	-1.128	11.806	6.396
β_V	-1.137	0.9676	0.079
H_R	-1.224	12.28	5.782
β_R	-1.420	1.384	0.094
$\Delta\beta$	-1.409	1.3614	-0.014
$H_V - H_R$	-0.689	2.853	0.598

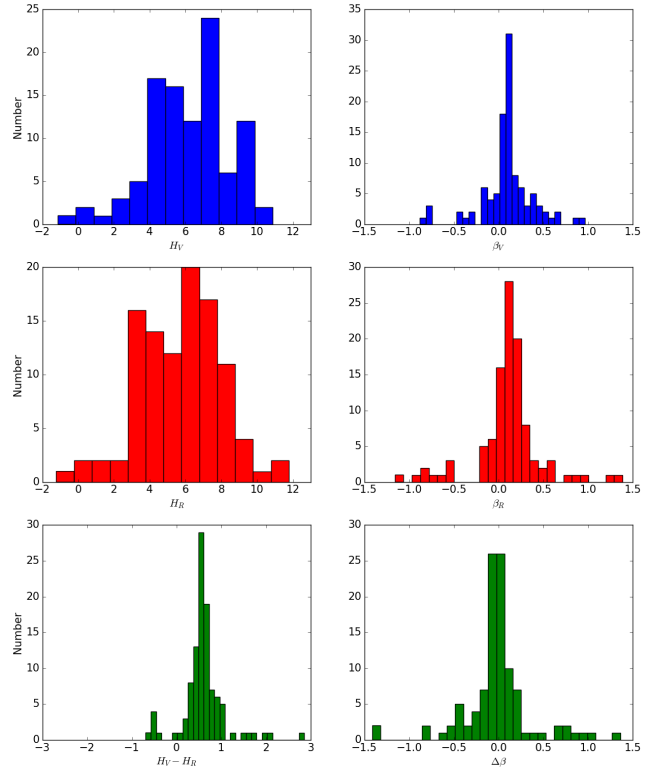


Figure 2. The histograms show the distributions of H_V and β_V (top), and H_R and β_R (bottom) of Sample [1].

as large as -1 mag per degree, are possible (see discussion below).

Most absolute colors are red, with a large concentration at $H_V - H_R \sim 0.6$, while $\Delta\beta = 0$ is the clear mode of its distribution, which is fairly symmetrical.

3.2 Search for correlations

We test our results (H_V , H_R , $H_V - H_R$, β_V , β_R , and $\Delta\beta$) for correlations among themselves and against other usual parameters, such as sizes, albedos, and orbital elements. We used the Spearman Correlation test that checks for the linear dependence between two ranked variables. It assesses monotonic relationships, whether linear or not.

The Spearman Correlation test provides two values, the

coefficient r_s and P_{r_s} . The first has the form:

$$r_s = 1 - \frac{6}{n(n^2 - 1)} \sum_{i=1}^n d_i^2, \quad (5)$$

where d_i is the difference of the assigned ranges between two variables, x_i and y_i , and n is the number of assigned pairs of data. Two pair of variables are correlated if $|r_s| \rightarrow 1$, while if $|r_s| \approx 0$ no correlation exists. The null hypothesis, that the two pair of variables are not correlated, is tested with P_{r_s} . In practice, the null hypothesis could be rejected if P_{r_s} tends to zero. In this work, we consider a correlation as significant if $|r_s| > 0.5$ and $P_{r_s} < 0.0015$ (significance over 3σ).

Our data includes all orbital sub-populations, from centaurs to detached objects (see Gladman 2008, for definitions). But for the sake of this work we will not analyze them separated as we consider that splitting our sample into smaller ones will only decrease its statistical reliability. Nevertheless, a small discussion is included in Sect. 4.

All the correlation results are reported in Table 3, where we marked in boldface those that are statistically significant. Among them the correlation between H_V (or H_R) and D (or p_V), should be simply explained by the relation between diameter, albedo, and absolute magnitude (Eq. 1).

As can be seen in Table 3, we used three separated samples: Sample [1], includes all objects in our database; Sample [2], includes only objects with H_V fainter than 4.5; and Sample [3], includes only objects with H_V brighter than 4.5 (see below for the justification).

Sample [1]:

It contains 114 objects with H_V and β_V , 113 with H_R and β_R , and 105 in common. Among them 64 objects have albedos and diameters reported by the *TNOs are cool* survey⁴.

The most interesting correlation that appears involves $H_V - H_R$ and $\Delta\beta$ (Fig. 3). The correlation clearly indicates that redder objects have smaller $\Delta\beta$. Physically, this means that, for redder surfaces, the phase curves in the R filter are steeper than the ones for the V filter, while the opposite holds for bluer objects.

Another feature of interest, but that has no significance as correlation, between $H_V - H_R$ and p_V , can be seen in Fig. 4. Lacerda et al. (2014) used a similar scatter plot (but using S' computed from average colors instead of absolute color) to propose that there exist two groups: one neutral and dark and other red and bright. Some weak evidence could be seen in our figure as well. We will come back to this issue further ahead.

Sub-samples by size ([2] and [3]):

Brown (2012) reported that the surface properties of objects with diameters larger than 500 km are different from smaller objects, for example due to volatile retention (e.g., Schaller & Brown 2007). Aiming at understanding if any size-related effect could be seen in our data we separated our objects into “small” (Sample [2]) and “large” (Sample [3]) according to $H_V = 4.5$.

Both sub-samples span more or less the same range in absolute colors and relative phase coefficient, with more extreme values in Sample [2], which seems reasonable due to the lower signal-to-noise ratio of the data. The most interesting feature is that the anti-correlation between $H_V - H_R$

Table 3. Correlation results. Parameters tested are shown in columns (1, 2), Spearman values (3, 4), and the confidence index CI, in terms of sigma, (5). N is the number of data points. Parameters tested: semi-major axis, a , eccentricity e , inclination i , visible albedo p_V , and diameter D . The brackets indicates the samples tested (see text).

P1	P2	r_s	P_{r_s}	CI	N	
H_V [1]	a	-0.4868	3.96×10^{-8}	(3σ)	114	
	e	0.2380	1.07×10^{-2}	(2σ)	114	
	i	-0.3913	1.66×10^{-5}	(3σ)	114	
	β_V	-0.1548	1.01×10^{-1}	(1σ)	114	
	D	-0.9808	1.69×10^{-46}	(3σ)	64	
	p_V	-0.5807	3.94×10^{-7}	(3σ)	64	
β_V	p_V	0.0031	9.74×10^{-1}	(< 1σ)	64	
	D	0.0215	8.26×10^{-1}	(< 1σ)	64	
H_R [1]	a	-0.4754	1.02×10^{-7}	(3σ)	113	
	e	0.2518	7.12×10^{-3}	(3σ)	113	
	i	-0.3584	9.67×10^{-5}	(3σ)	113	
	β_R	-0.1652	8.01×10^{-2}	(1σ)	113	
	D	-0.9630	1.33×10^{-37}	(3σ)	64	
	p_V	-0.6389	1.02×10^{-8}	(3σ)	64	
β_R	p_V	-0.0730	4.59×10^{-1}	(1σ)	64	
	D	0.0098	9.20×10^{-1}	(< 1σ)	64	
$H_V - H_R$ [1]	$\Delta\beta$	-0.8117	8.295×10^{-26}	(3σ)	105	
	a	0.0377	7.018×10^{-01}	(< 1σ)	105	
	e	-0.0054	9.558×10^{-01}	(< 1σ)	105	
	i	-0.1697	8.34×10^{-02}	(1σ)	105	
	H_V	0.1364	1.651×10^{-01}	(1σ)	105	
	H_R	-0.0382	6.987×10^{-01}	(< 1σ)	105	
	D	-0.1016	4.204×10^{-01}	(< 1σ)	64	
	p_V	0.2224	6.21×10^{-02}	(< 1σ)	64	
	$\Delta\beta$ [1]	a	-0.0074	9.397×10^{-01}	(< 1σ)	105
		e	0.0526	5.935×10^{-01}	(< 1σ)	105
		i	0.0172	8.613×10^{-01}	(< 1σ)	105
H_V		-0.0793	4.213×10^{-01}	(< 1σ)	105	
H_R		0.0766	4.370×10^{-01}	(< 1σ)	105	
	D	0.0475	7.069×10^{-01}	(< 1σ)	64	
	p_V	-0.0892	4.796×10^{-01}	(< 1σ)	64	
H_V [2]	D	-0.9661	1.01×10^{-28}	(3σ)	47	
	p_V	-0.4070	4.09×10^{-3}	(3σ)	47	
β_V [2]	D	0.0753	6.1×10^{-01}	(< 1σ)	47	
	p_V	-0.2096	1.5×10^{-01}	(1σ)	47	
H_R [2]	D	-0.9467	2.81×10^{-24}	(3σ)	47	
	p_V	-0.4807	5.42×10^{-4}	(3σ)	47	
β_R [2]	D	0.3261	2.36×10^{-02}	(3σ)	47	
	p_V	0.0736	6.18×10^{-01}	(1σ)	47	
$H_V - H_R$ [2]	$\Delta\beta$	-0.7912	3.34×10^{-19}	(3σ)	84	
	H_V	0.0204	8.53×10^{-1}	(< 1σ)	84	
	H_R	-0.1999	6.82×10^{-2}	(1σ)	84	
	D	0.2058	1.60×10^{-1}	(1σ)	47	
	p_V	0.5912	9.63×10^{-6}	(3σ)	47	
	$\Delta\beta$ [2]	H_V	0.0710	5.2×10^{-1}	(< 1σ)	84
H_R		0.2652	1.47×10^{-2}	(2σ)	84	
D		-0.3368	1.92×10^{-2}	(2σ)	47	
p_V		-0.3769	8.2×10^{-3}	(3σ)	47	
H_V [3]	D	-0.8504	1.52×10^{-05}	(3σ)	17	
	p_V	-0.6412	5.53×10^{-03}	(3σ)	17	
β_V	D	0.0948	6.826×10^{-01}	(1σ)	17	
	p_V	0.0955	6.801×10^{-01}	(1σ)	17	
H_R [3]	D	-0.7401	6.79×10^{-04}	(3σ)	17	
	p_V	-0.7862	1.82×10^{-04}	(3σ)	17	
β_R	D	-0.2583	2.580×10^{-01}	(1σ)	17	
	p_V	-0.1197	6.051×10^{-01}	(1σ)	17	
$H_V - H_R$ [3]	$\Delta\beta$	-0.8986	3.15×10^{-08}	(3σ)	21	
	H_V	0.4204	5.77×10^{-02}	(1σ)	21	
	H_R	-0.0045	9.84×10^{-01}	(< 1σ)	21	
	D	-0.3872	1.24×10^{-01}	(1σ)	17	
	p_V	-0.3243	2.04×10^{-01}	(1σ)	17	
	$\Delta\beta$ [3]	H_V	-0.4840	2.61×10^{-02}	(3σ)	21
H_R		-0.0708	7.603×10^{-1}	(< 1σ)	21	
D		0.3725	1.408×10^{-1}	(1σ)	17	
p_V		0.3636	1.513×10^{-1}	(1σ)	17	

⁴ <http://public-tnosarecool.lesia.obspm.fr>

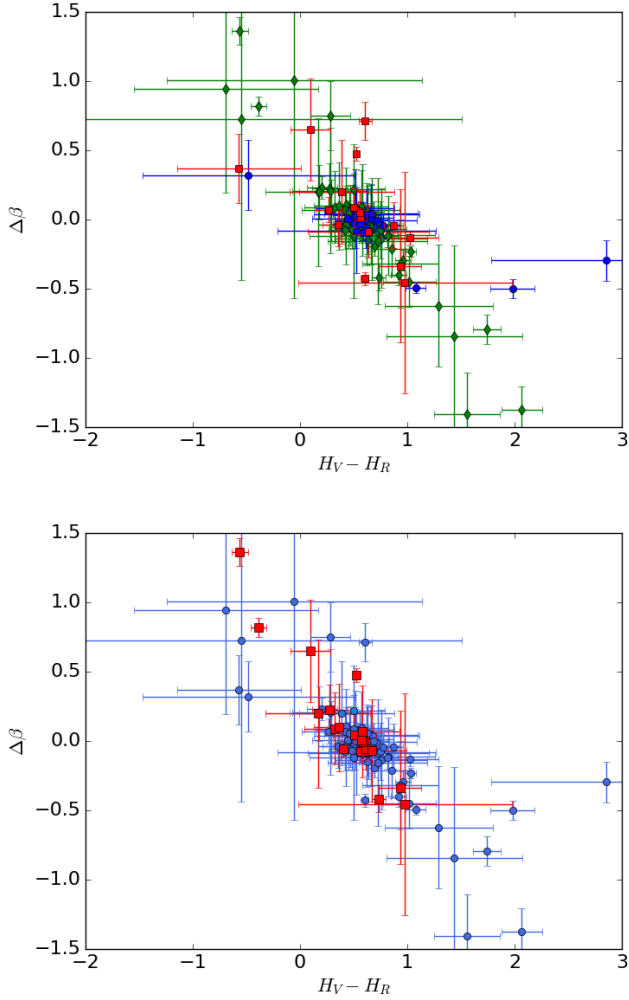


Figure 3. Scatter plot of $H_V - H_R$ and $\Delta\beta$. The top panel shows Sample [1] in bins of semi-major axis color-coded as: $a < 40$ AU in blue dots, $40 < a < 50$ AU in green diamonds, $a > 50$ AU in red squares. The bottom panel shows Sample [2] in blue dots and Sample [3] in red squares.

and $\Delta\beta$ holds for both sub-samples indicating, perhaps, that it is related to surface properties rather than size. Also, as objects from all regions of the trans-Neptunian belt are included (centaurs as well), the correlation is possibly not due to some unknown observational bias (Fig. 3).

Sample [2] (Sample [3]) include 84 (21) objects with V and R data, 47 (17) of which have *TNOs are cool* diameters and albedos. Sample [2] has on average lower albedos than Sample [3] (Fig. 5, bottom panel), which is expected due to the retention of volatiles on the larger objects. For Sample [2] the absolute color is correlated with the albedo, implying that high albedo surfaces (with an upper limit in size of 500 km) have redder colors, while no similar correlation is seen among Sample [3].

In general, there exists a trend on higher absolute magnitudes H_V (and H_R) and albedo. We did not use p_R , that could have been computed using $H_V - H_R$ and the albedo, as

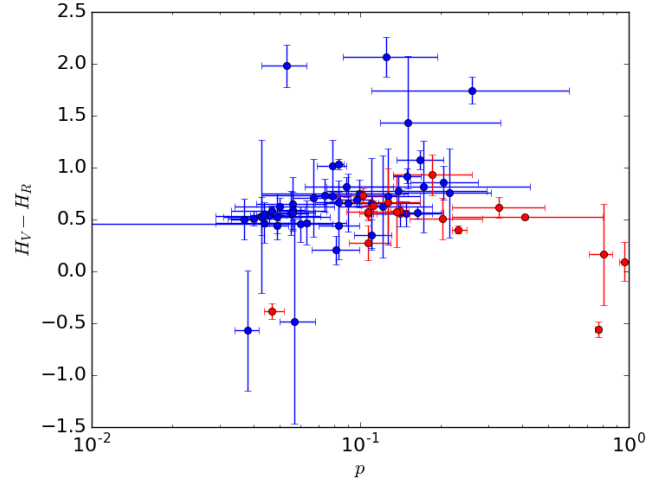


Figure 4. Scatter plot of $H_V - H_R$ vs. p_V . Sample [2] is shown in blue dots, while Sample [3] is represented with red dots.

it would not have been a quantity obtained independently from our data.

4 DISCUSSION AND CONCLUSIONS

In this paper we present H_V (β_V) for 114 objects and H_R (β_R) for 113. These results were obtained from data observed by ourselves and from the literature. Note that 105 objects have both phase curves and therefore absolute colors. In paper 1 we had not included data in the R filter, thus the present work expands our previous results. We tested for different correlations, among our data, orbital parameters, and data from the *TNOs are cool* survey.

The most interesting correlation we found is between $H_V - H_R$ and $\Delta\beta$. The correlation holds if we consider different bins in semi-major axis (see Fig. 3, top) and separate between large and small objects (Fig. 3, bottom). Therefore, we conclude it is intrinsic to the TNO (and associated) population. This correlation indicates that redder objects have steeper phase curves in the R filter than in the V filter, while the opposite is true for bluer objects. As many different surfaces types, sizes, and dynamical evolutions are being sampled by our absolute colors we cannot assure that we are seeing an evolutionary effect, but probably something related to the porosity and compaction of the surfaces. The intrinsic brightness of the object depends of asteroid albedo, which is determined by the surface composition, compaction and grains size. There is a dependence of phase coefficient on surface texture (Shkuratov 1994,b). However, given the inhomogenities of our data base, further studies are needed to clarify this interpretation.

We separated our sample into two sub-groups: large and small, using $H_V = 4.5$ as discriminant based on the results of Brown (2012) in order to use all our dataset. Interestingly, there seems to be a gap in this region (Fig. 5 top) which remains to be confirmed. From our search for correlations among the two aforementioned groups (large and small) we found that:

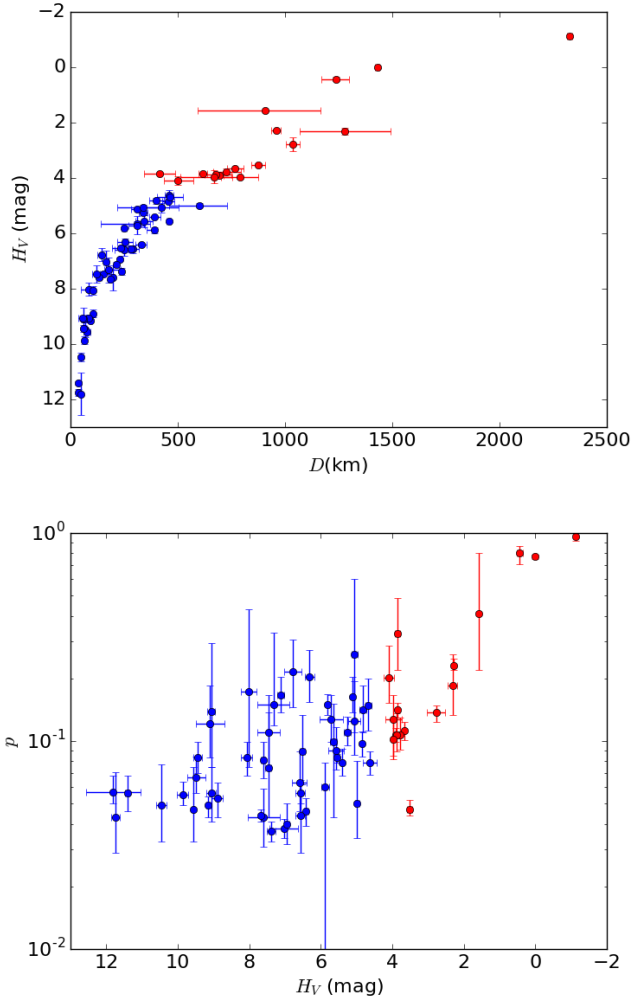


Figure 5. Scatter plot of H_V vs. D (top) and H_V vs. p_V (bottom). Samples [2] and [3] are shown in different colors, blue the former and red the latter.

- The correlation between $H_V - H_R$ and $\Delta\beta$ holds for both of them. As we do not expect the surface composition to be the same in both groups (in fact it is clear that the large objects do not have objects as red as the small population) and the albedo distributions are different, we consider that the correlation is due to surface micro-structure (compaction, grain size) in a yet-to-be-understood way. Surface temperature does not seem to be a key factor here either, at least in first approximation, as the correlation holds for different bins in semi-major axis as well.

- There exists a significant correlation between $H_V - H_R$ and p_V for the small objects (upper size limit at ~ 500 km). According to this correlation the redder objects have higher albedos. For the larger objects there is a marginal (opposite) trend.

- Regarding the small objects, the high-albedo tend, as well, to be the larger objects as shown in Fig. 5. According to our understanding of collisional and resurfacing models, an initially neutral bright surface (ice-covered) under irradiation will decrease its albedo in the visible faster than in the

red. Further irradiation will decrease the albedo in the red letting a dark carbon-covered surface with a neutral slope (e.g., Strazzulla et al. 1991; Thompson et al. 1987; Hudson et al. 2008, and references). The main opposing mechanism is collisional, that craterize the surface exposing sub-superficial material (see Gil-Hutton 2002). Therefore, the larger “small” objects, of higher albedo and red, are probably well processed, but not yet in the last stages of irradiation, while the smaller, bluer and lower-albedo, could be objects that are very processed. This is very curious, because these smaller objects (Fig. 6-right) should have suffered more impacts than larger ones (e.g., Dohnanyi 1971; Farinella & Davis 1992) and, in principle, there should be at least some objects with higher albedos.

We also searched for correlations among the different dynamical classes: Centaurs, Classical TNOs, Scattering objects (including Detached objects, and Resonant objects, following Gladman (2008). Although with a lower number of objects, the correlation between $H_V - H_R$ and $\Delta\beta$ appears in all subpopulations, pointing even more towards a property shared by all these minor bodies and that deserves further analysis.

Following part of the discussion drawn in paper 1, it becomes clear that, although the β distribution are clearly unimodal and that about 60 % of the objects are close to the mode of the distribution, a non-negligible fraction of objects have values that can differ by a significant amount of the mode. Therefore an “average” value of the phase coefficient must be taken, and used, with extreme caution.

A phase curve with negative values of β do not have a direct physical interpretation in terms of photometric models, see our discussion in paper 1. Nevertheless, some plausible explanations are (i) underestimation of rotational amplitude, which could account for values of reduced magnitudes different than expected by our simple model (Eq. 4), (ii) the presence of material surrounding the body (ring systems, satellites, or binaries) which modify the total reflecting area as seen from Earth, and (iii) faint cometary-like activity. Further deeper, in quality and quantity, photometric studies are needed in order to discern between these scenarios.

The absolute magnitudes and phase coefficients have been obtained from heterogeneous sources, with a variety of precisions, from a wide distribution of telescopes, instruments, and filters. Nevertheless, we have used homogeneous techniques to analyze them and produce an accurate database, although probably not as precise as desired, especially due to the large uncertainties introduced by unknown rotational properties. Also, our results are, in a way, mean values, as observations covering large intervals of time are being used here and some objects are known to suffer changes in relatively short time-scales, for instance the ring bearer Chariklo. Nevertheless, the statistical significance of our database is robust and we intend to continue increasing it, including new observations reported in the literature and our own forthcoming observations.

ACKNOWLEDGMENTS

We are very grateful to the anonymous referee for valuable comments which helped us to improve this paper. Based in part on observations collected at the German-Spanish

Astronomical Center, Calar Alto, operated jointly by Max-Planck- Institut für Astronomie and Instituto de Astrofísica de Andalucía (CSIC). Partially based on observations obtained at the Southern Astrophysical Research (SOAR) telescope, which is a joint project of the Ministério da Ciência, Tecnologia, e Inovação (MCTI) da República Federativa do Brasil, the U.S. National Optical Astronomy Observatory (NOAO), the University of North Carolina at Chapel Hill (UNC), and Michigan State University (MSU). CAL acknowledges support from CNPq. AAC acknowledges support from CNPq and FAPERJ. Part of the research leading to these results has received funding from the European Union's Horizon 2020 Research and Innovation Programme, under Grant Agreement No. 687378. PSS and JLO would like to acknowledge financial support by the Spanish grant AYA-2014-56637-C2-1-P and the Proyecto de Excelencia de la Junta de Andalucía J.A. 2012-FQM1776.

REFERENCES

- Alvarez-Candal, A., Pinilla-Alonso, N., Ortiz, J. L., et al. 2016, *A&A*, 586, A155
- Barucci, M. A., Romon, J., Le Bras, A., Fulchignoni, M., & Tholen, D. 1999, AAS/Division for Planetary Sciences Meeting Abstracts #31, 31, 23.04
- Barucci, M. A., Cruikshank, D. P., Dotto, E., et al. 2005, *Bulletin of the American Astronomical Society*, 37, 56.01
- Barucci, M. A., Alvarez-Candal, A., Merlin, F., et al. 2011, EPSC-DPS Joint Meeting 2011, 473
- Belskaya, I. N., & Shevchenko, V. G. 2000, *Icarus*, 147, 94
- Belskaya, I. N., & Shevchenko, V. G. 2000, *Icarus*, 147, 94
- Benecchi, S. D., & Sheppard, S. S. 2013, *AJ*, 145, 124
- Boehnhardt, H., Tozzi, G. P., Birkle, K., et al. 2001, *A&A*, 378, 653
- Boehnhardt, H., Delsanti, A., Hainaut, O., et al. 2002, *Asteroids, Comets, and Meteors: ACM 2002*, 500, 47
- Boehnhardt, H., Bagnulo, S., Muinonen, K., et al. 2004, *A&A*, 415, L21
- Dohnanyi, J. S. 1971, *NASA Special Publication*, 263.
- Brown, M. E. 2012, *Annual Review of Earth and Planetary Sciences*, 40, 467
- Carraro, G., Maris, M., Bertin, D., & Parisi, M. G. 2006, *A&A*, 460, L39
- Carry, B., Snodgrass, C., Lacerda, P., Hainaut, O., & Dumas, C. 2012, *A&A*, 544, A137
- Delsanti, A. C., Boehnhardt, H., Barrera, L., & Hainaut, O. R. 2001, *Bulletin of the American Astronomical Society*, 33, 12.04
- Doressoundiram, A., Boehnhardt, H., Tegler, S. C., & Trujillo, C. 2008, *The Solar System Beyond Neptune*, 91
- Farinella P., Davis D. R., 1992, *Icar*, 97, 111
- Galiazzo, M., de la Fuente Marcos, C., de la Fuente Marcos, R., et al. 2016, *Ap&SS*, 361, 212
- Gil-Hutton, R. 2002, *Planet. Space Science*, 50, 57
- Gladman, B. 2008, *Bulletin of the American Astronomical Society*, 40, 7.03
- Hicks, M. D., Simonelli, D. P., & Buratti, B. J. 2005, *Icarus*, 176, 492
- Hudson, P. K., Young, M. A., Kleiber, P. D., & Grassian, V. H. 2008, *Atmospheric Environment*, 42, 5991
- Jewitt, D., Aussen, H., & Evans, A. 2001, *Nature*, 411, 446
- Jewitt, D. 2015, *AJ*, 150, 201
- Kaňuchová, Z., Brunetto, R., Melita, M., et al. 2012, *Icarus*, 221, 12.
- Landolt, A. U. 1992, *AJ*, 104, 340
- Lacerda, P., Fornasier, S., Lellouch, E., et al. 2014, *ApJ*, 793, L2
- Luu, J. & Jewitt, D. 1996, *AJ*, 112, 2310.
- Muinonen, K., Belskaya, I. N., Cellino, A., et al. 2010, *Icarus*, 209, 542
- Muinonen, K., Tyynelä, J., Zubko, E., et al. 2010, *Earth, Planets, and Space*, 62, 47.]
- Mueller, T. G., Lellouch, E., Boehnhardt, H., et al. 2010, *European Planetary Science Congress 2010*, 668
- Peixinho, N., Delsanti, A., Guilbert-Lepoutre, A., Gafeira, R., & Lacerda, P. 2012, *A&A*, 546, A86
- Pike, R. E., Fraser, W. C., Schwamb, M. E., et al. 2017, *AAS/Division for Planetary Sciences Meeting Abstracts 49*, 504.12.
- Rabinowitz, D. L., Schaefer, B. E., & Tourtellotte, S. W. 2007, *AJ*, 133, 26
- Roig, F., Ribeiro, A. O. & Gil-Hutton, R. 2008, *A&A*, 483, 911
- Rousselot, P., Petit, J.-M., Poulet, F., & Sergeev, A. 2005, *Icarus*, 176, 478
- Santos-Sanz, P., Ortiz, J. L., Barrera, L., & Boehnhardt, H. 2009, *A&A*, 494, 693
- Schaller, E. L., & Brown, M. E. 2007, *European Planetary Science Congress 2007*, 699
- Sheppard, S. S., & Jewitt, D. C. 2002, *AJ*, 124, 1757
- Shkuratov, Y., Ovcharenko, A., Zubko, E., et al. 2002, *Icarus*, 159, 396
- Shkuratov, Y. G. 1994, *Solar System Research*, 28, 77.
- Shkuratov, Y. G. 1994b, *Astronomicheskii Vestnik*, 28, 155.
- Snodgrass, C., Carry, B., Dumas, C., & Hainaut, O. 2010, *European Planetary Science Congress 2010*, 423
- Strazzulla, G., Baratta, G. A., Johnson, R. E., & Donn, B. 1991, *Icarus*, 91, 101
- Tegler, S. C., Romanishin, W., & Consolmagno, G. J. 2003, *ApJ*, 599, L49
- Thirouin, A., Ortiz, J. L., Duffard, R., et al. 2010, *VizieR Online Data Catalog*, 352
- Thirouin, A., Ortiz, J. L., Campo Bagatin, A., et al. 2012, *MNRAS*, 424, 3156
- Thompson, W. R., Henry, T., Khare, B. N., Flynn, L., & Schwartz, J. 1987, *J. Geophys. Res.*, 92, 15083

This paper has been typeset from a $\text{\TeX}/\text{\LaTeX}$ file prepared by the author.

Table 4. Absolute Magnitudes

Object	H_V (mag)	β_V (mag per degree)	N_V	H_R (mag)	β_R (mag per degree)	N_R	Δm	Ref.
15760 1992 QB ₁	7.83 ± 0.05	-0.193 ± 0.05	3	6.87 ± 0.05	0.102 ± 0.05	3	0.04	Al16
15788 1993 SB	7.99 ± 0.18	0.373 ± 0.13	5	7.70 ± 0.20	0.307 ± 0.17	4	0.14	Al16
15789 1993 SC	7.39 ± 0.02	0.050 ± 0.01	8	6.71 ± 0.02	0.015 ± 0.02	6	0.04	Al16
1994 EV ₃₃	8.18 ± 0.12	-0.801 ± 0.19	3	7.75 ± 0.11	-0.907 ± 0.18	3	0.14	Al16
16684 1994 JQ ₁	7.03 ± 0.14	0.568 ± 0.18	5	6.75 ± 0.11	-0.181 ± 0.17	5	0.14	Al16
1994 TB	8.01 ± 0.22	0.132 ± 0.15	9	7.19 ± 0.37	0.247 ± 0.23	7	0.34	Al16
1994 VK ₈	7.83 ± 0.91	-0.174 ± 0.97	3	0.42	Al16
1995 HM ₅	8.31 ± 0.08	0.037 ± 0.08	5	7.89 ± 0.17	-0.032 ± 0.12	4	0.14	Al16
1995 QY ₉	8.13 ± 0.53	-0.110 ± 0.53	3	0.60	Al16
24835 1995 SM ₅₅	4.58 ± 0.17	0.137 ± 0.19	7	4.15 ± 0.18	0.177 ± 0.20	7	0.19	Al16
26181 1996 GQ ₂₁	5.07 ± 0.04	0.857 ± 0.12	6	4.46 ± 0.02	0.144 ± 0.05	9	0.14	Al16, TW
1996 RQ ₂₀	6.97 ± 0.08	0.56 ± 0.10	4	6.67 ± 0.29	0.269 ± 0.26	4	0.14	Al16
1996 RR ₂₀	6.98 ± 0.18	0.391 ± 0.19	3	6.40 ± 0.17	0.297 ± 0.18	3	0.14	Al16
19299 1996 SZ ₄	8.56 ± 0.08	0.306 ± 0.07	4	8.04 ± 0.08	0.308 ± 0.07	3	0.14	Al16
1996 TK ₆₆	7.02 ± 0.20	-0.278 ± 0.22	3	6.52 ± 0.20	-0.499 ± 0.22	3	0.14	Al16
15874 1996 TL ₆₆	5.25 ± 0.09	0.375 ± 0.11	5	4.90 ± 0.10	0.414 ± 0.10	3	0.12	Al16
19308 1996 TO ₆₆	4.81 ± 0.19	0.174 ± 0.23	10	4.31 ± 0.36	0.291 ± 0.38	8	0.14	JL01, Se02, Al16, TW
15875 1996 TP ₆₆	7.46 ± 0.08	0.126 ± 0.07	5	6.73 ± 0.13	0.199 ± 0.09	3	0.14	Al16
118228 1996 TQ ₆₆	8.00 ± 0.42	-0.414 ± 0.67	4	0.14	Al16
1996 TS ₆₆	6.53 ± 0.16	0.084 ± 0.21	4	0.14	Da00, JL01, JL98, RT99
33001 1997 CU ₂₉	6.80 ± 0.07	0.075 ± 0.12	4	6.15 ± 0.07	0.133 ± 0.12	4	0.14	Al16
1997 QH ₄	7.21 ± 0.25	0.450 ± 0.22	4	6.27 ± 0.25	0.766 ± 0.22	4	0.14	Al16
24952 1997 QJ ₄	7.75 ± 0.11	0.290 ± 0.10	5	7.26 ± 0.11	0.357 ± 0.10	4	0.14	Al16
33128 1998 BU ₄₈	5.71 ± 2.00	0.967 ± 1.12	4	6.26 ± 0.47	0.244 ± 0.26	12	0.68	Al16, TW
91133 1998 HK ₁₅₁	7.33 ± 0.05	0.127 ± 0.08	5	6.87 ± 0.07	0.071 ± 0.10	5	0.14	Al16
385194 1998 KG ₆₂	7.64 ± 0.10	-0.747 ± 0.13	3	7.01 ± 0.10	-0.803 ± 0.13	3	0.14	Al16
85633 1998 KR ₆₅	-1.91 ± 1.43	7.187 ± 1.21	3	0.14	Bo02, TR03
26308 1998 SM ₁₆₅	5.93 ± 0.36	0.448 ± 0.37	3	0.14	Al16
35671 1998 SN ₁₆₅	5.87 ± 0.10	-0.031 ± 0.11	6	5.42 ± 0.12	0.005 ± 0.12	5	0.14	Al16
1998 UR ₄₃	9.04 ± 0.11	-0.763 ± 0.20	3	8.42 ± 0.11	-0.728 ± 0.21	3	0.14	Al16
33340 1998 VG ₄₄	6.60 ± 0.20	0.226 ± 0.15	3	6.13 ± 0.05	0.145 ± 0.05	5	0.10	Se02, Al16, TW
1999 CD ₁₅₈	5.28 ± 0.23	0.092 ± 0.30	3	5.00 ± 0.26	-0.114 ± 0.33	3	0.14	Al16
26375 1999 DE ₉	5.11 ± 0.02	0.182 ± 0.03	36	4.55 ± 0.05	0.167 ± 0.04	11	0.10	Se02, Al16, TW
1999 HS ₁₁	6.84 ± 0.86	0.227 ± 1.12	3	6.90 ± 0.81	-0.779 ± 1.10	3	0.14	Al16
40314 1999 KR ₁₆	6.31 ± 0.13	-0.124 ± 0.18	4	5.46 ± 0.07	0.091 ± 0.07	15	0.18	Al16, TW
44594 1999 OX ₃	7.60 ± 0.06	0.108 ± 0.04	14	7.40 ± 0.12	-0.122 ± 0.07	19	0.11	BA03, Th12, Al16, TW
86047 1999 OY ₃	6.44 ± 0.13	0.272 ± 0.15	3	6.26 ± 0.12	0.075 ± 0.11	5	0.14	Al16
1999 RY ₂₁₅	6.60 ± 0.10	0.429 ± 0.13	3	0.14	Bo02, Do01, Sn10
47171 1999 TC ₃₆	5.39 ± 0.02	0.110 ± 0.02	45	4.67 ± 0.03	0.195 ± 0.03	7	0.070	Al16
29981 1999 TD ₁₀	9.09 ± 0.38	0.036 ± 0.11	27	8.45 ± 0.40	0.122 ± 0.15	16	0.650	Ro03, Mu04, Al16
121725 1999 XX ₁₄₃	9.09 ± 0.27	0.066 ± 0.20	4	8.57 ± 0.24	-0.012 ± 0.19	4	0.14	BA03, Al16, TW
47932 2000 GN ₁₇₁	6.77 ± 0.24	-0.100 ± 0.18	30	6.01 ± 0.35	0.035 ± 0.30	13	0.61	SJ02, Ca12, Al16, TW
138537 2000 OK ₆₇	6.63 ± 0.86	0.087 ± 0.65	3	0	0.14	Al16
82075 2000 YW ₁₃₄	4.38 ± 0.68	0.373 ± 0.55	3	3.40 ± 0.72	0.832 ± 0.58	3	0.10	Al16
63252 2001 BL ₄₁	11.74 ± 0.12	0.027 ± 0.03	4	11.21 ± 0.13	0.033 ± 0.03	4	0.14	Al16, TW
150642 2001 CZ ₃₁	5.54 ± 0.14	0.111 ± 0.16	3	0.21	SJ02
82158 2001 FP ₁₈₅	6.40 ± 0.06	0.140 ± 0.04	6	5.87 ± 0.05	0.078 ± 0.04	7	0.06	Al16, TW
82155 2001 FZ ₁₇₃	6.12 ± 0.08	0.339 ± 0.08	4	5.62 ± 0.09	0.253 ± 0.10	6	0.06	SJ02, Al16, TW
2001 KA ₇₇	5.64 ± 0.09	0.130 ± 0.11	3	4.89 ± 0.09	0.206 ± 0.16	3	0.14	Al16
2001 KD ₇₇	6.52 ± 0.07	-0.005 ± 0.06	4	5.71 ± 0.06	0.111 ± 0.05	4	0.07	Al16
2001 QC ₂₉₈	6.06 ± 0.10	0.331 ± 0.1	3	0.14	Sn10, SS09, TW
2001 QY ₂₉₇	5.50 ± 0.24	-0.295 ± 0.2	7	0.49	Th12, TW
42301 2001 UR ₁₆₃	4.52 ± 0.06	0.363 ± 0.11	3	3.65 ± 0.06	0.404 ± 0.11	3	0.08	Al16
55565 2002 AW ₁₉₇	3.65 ± 0.02	0.077 ± 0.03	38	3.02 ± 0.04	0.151 ± 0.06	4	0.04	Al16
2002 GP ₃₂	7.13 ± 0.02	-0.134 ± 0.03	4	6.53 ± 0.02	0.292 ± 0.02	4	0.03	Al16
95626 2002 GZ ₃₂	7.38 ± 0.12	0.072 ± 0.05	30	6.88 ± 0.15	0.106 ± 0.06	5	0.15	Al16
2002 KW ₁₄	6.34 ± 0.40	-1.420 ± 0.37	5	0.25	Th12, TW
119951 2002 KX ₁₄	4.83 ± 0.03	0.277 ± 0.03	21	4.14 ± 0.04	0.468 ± 0.06	5	0.05	Re13 Al16
250112 2002 KY ₁₄	11.80 ± 0.76	-0.273 ± 0.19	4	12.28 ± 0.62	-0.593 ± 0.16	4	0.13	Al16
2002 PN ₃₄	8.61 ± 0.05	0.089 ± 0.02	57	0.18	Al16

Table 4. Absolute Magnitudes

Object	H_V (mag)	β_V (mag per degree)	N_V	H_R (mag)	β_R (mag per degree)	N_R	Δm	Ref.
55637 2002 UX ₂₅	3.90 ± 0.04	0.104 ± 0.05	46	3.34 ± 0.05	0.176 ± 0.06	17	0.21	All16, TW
55638 2002 VE ₉₅	5.81 ± 0.03	0.088 ± 0.02	43	4.89 ± 0.06	0.487 ± 0.07	4	0.08	All16
127546 2002 XU ₉₃	7.03 ± 0.40	0.496 ± 0.17	5	7.60 ± 0.41	0.125 ± 0.17	5	0.14	All16
208996 2003 AZ ₈₄	3.77 ± 0.11	0.074 ± 0.11	5	3.49 ± 0.11	-0.151 ± 0.13	5	0.14	All16
120061 2003 CO ₁	9.14 ± 0.05	0.092 ± 0.01	5	8.70 ± 0.05	0.084 ± 0.01	5	0.07	All16
133067 2003 FB ₁₂₈	6.92 ± 0.60	0.422 ± 0.53	3	7.61 ± 0.60	-0.519 ± 0.52	3	0.14	All16
2003 FE ₁₂₈	7.38 ± 0.34	-0.348 ± 0.29	5	6.08 ± 0.36	0.274 ± 0.32	5	0.14	All16
120132 2003 FY ₁₂₈	4.63 ± 0.18	0.534 ± 0.14	7	3.61 ± 0.16	0.983 ± 0.11	6	0.15	All16
385437 2003 GH ₅₅	7.31 ± 0.44	-0.878 ± 0.46	3	5.88 ± 0.44	-0.034 ± 0.46	3	0.14	All16
120178 2003 OP ₃₂	4.05 ± 0.21	0.056 ± 0.19	10	3.73 ± 0.17	-0.033 ± 0.16	9	0.18	All16
2003 QW ₉₀	6.35 ± 0.45	-1.137 ± 0.51	3	0.14	All16
2003 UY ₁₁₇	5.60 ± 0.10	0.280 ± 0.11	3	0.14	All16
416400 2003 UZ ₁₁₇	5.23 ± 0.10	0.133 ± 0.10	5	4.81 ± 0.11	0.209 ± 0.09	4	0.14	All16
2003 UZ ₄₁₃	4.36 ± 0.17	0.143 ± 0.22	3	3.99 ± 0.16	0.044 ± 0.22	3	0.14	All16
136204 2003 WL ₇	8.89 ± 0.14	0.088 ± 0.04	4	6.91 ± 0.14	0.588 ± 0.04	3	0.05	All16
120216 2004 EW ₉₅	6.57 ± 0.13	0.080 ± 0.09	5	6.10 ± 0.13	0.135 ± 0.09	5	0.14	All16
307982 2004 PG ₁₁₅	4.95 ± 0.45	0.445 ± 0.34	8	4.56 ± 0.17	0.243 ± 0.14	9	0.14	All16, TW
2004 PT ₁₀₇	6.33 ± 1.02	-0.347 ± 0.76	3	0.14	All16
2004 TY ₃₆₄	4.51 ± 0.13	0.145 ± 0.10	32	0.22	All16
144897 2004 UX ₁₀	4.82 ± 0.09	0.060 ± 0.10	8	4.26 ± 0.07	0.062 ± 0.07	8	0.08	All16
230965 2004 XA ₁₉₂	5.05 ± 0.08	-0.174 ± 0.07	5	3.31 ± 0.09	0.620 ± 0.07	6	0.07	All16, TW
2005 GE ₁₈₇	7.13 ± 0.18	0.065 ± 0.13	3	0.14	Ca12, TW
2005 QU ₁₈₂	3.85 ± 0.06	0.277 ± 0.10	5	3.23 ± 0.06	0.336 ± 0.10	5	0.12	All16
2005 RM ₄₃	4.70 ± 0.08	-0.027 ± 0.06	6	4.44 ± 0.08	-0.098 ± 0.06	5	0.04	All16
2005 RN ₄₃	3.88 ± 0.05	0.139 ± 0.04	11	3.30 ± 0.03	0.133 ± 0.03	10	0.06	Re13, All16, TW
2005 RR ₄₃	4.25 ± 0.06	-0.003 ± 0.06	5	3.75 ± 0.06	0.160 ± 0.06	4	0.06	Re13, All16
2005 TB ₁₉₀	4.67 ± 0.08	0.051 ± 0.10	8	4.12 ± 0.08	-0.001 ± 0.11	12	0.12	All16, TW
2005 UQ ₅₁₃	4.09 ± 0.14	-0.130 ± 0.14	3	3.58 ± 0.13	-0.174 ± 0.13	4	0.06	Sn10, All16*, TW
2007 OC ₁₀	5.70 ± 0.32	-0.115 ± 0.32	4	4.98 ± 0.32	0.042 ± 0.32	4	0.14	All16, TW
2007 OR ₁₀	2.31 ± 0.13	0.255 ± 0.34	7	1.38 ± 0.14	0.590 ± 0.43	4	0.09	All16
2008 FC ₇₆	9.48 ± 0.26	0.101 ± 0.05	3	8.77 ± 0.26	0.110 ± 0.05	4	0.14	All16
2008 OG ₁₉	6.46 ± 0.19	-1.787 ± 0.17	4	0.14	TW
2013 AZ ₆₀	10.4 ± 0.19	0.030 ± 0.03	3	9.43 ± 0.19	0.164 ± 0.03	3	0.14	All16
55576 Amycus	8.07 ± 0.16	0.127 ± 0.05	5	7.41 ± 0.13	0.113 ± 0.04	5	0.16	BA03, All16, TW
8405 Asbolus	9.06 ± 0.13	0.072 ± 0.03	43	8.41 ± 0.21	0.155 ± 0.06	6	0.55	BA03, All16, TW
54598 Bienor	7.59 ± 0.45	0.188 ± 0.19	59	7.06 ± 0.58	0.267 ± 0.24	5	0.75	BA03, All16, TW
Borasisi	6.03 ± 0.03	0.23 ± 0.06	3	0.05	BA03, All16, TW
65489 Ceto	6.57 ± 0.12	0.195 ± 0.09	9	5.98 ± 0.12	0.209 ± 0.09	10	0.13	All16, TW
19521 Chaos	4.98 ± 0.06	0.102 ± 0.07	6	4.36 ± 0.04	0.254 ± 0.06	7	0.10	SJ02, All16, TW
10199 Chariklo	6.94 ± 0.05	0.049 ± 0.01	21	6.42 ± 0.04	0.021 ± 0.01	35	0.10	Ga16, BA03, All16, TW
2060 Chiron	7.11 ± 0.08	-0.410 ± 0.03	8	6.04 ± 0.02	0.080 ± 0.00	54	0.09	Ga16, BA03, All16, TW
83982 Crantor	9.09 ± 0.40	0.109 ± 0.14	6	8.47 ± 0.28	0.074 ± 0.10	5	0.34	BA03, All16, TW
52975 Cyllarus	9.06 ± 0.10	0.171 ± 0.06	6	8.29 ± 0.10	0.218 ± 0.06	6	0.14	BA03, All16, TW
60558 Echeclus	9.86 ± 0.14	0.056 ± 0.05	11	9.30 ± 0.14	0.076 ± 0.05	13	0.24	BA03, Ro05, TW
31824 Elatus	10.46 ± 0.14	0.088 ± 0.02	13	9.93 ± 0.16	0.059 ± 0.03	16	0.24	BA02, All16, TW
136199 Eris	-1.12 ± 0.02	0.135 ± 0.05	76	-1.22 ± 0.18	-0.516 ± 0.36	9	0.10	DM09, Ra07, Ca06, All16, TW
136108 Haumea	0.43 ± 0.07	0.101 ± 0.09	90	0.26 ± 0.48	-0.095 ± 0.52	5	0.29	Ra06, All16
38628 Huya	5.55 ± 0.04	-0.152 ± 0.03	45	4.52 ± 0.02	0.078 ± 0.01	104	0.10	BA03, Bo04, Ga16, SJ02, All16
10370 Hylonome	9.57 ± 0.02	0.079 ± 0.01	6	8.98 ± 0.04	0.173 ± 0.02	5	0.04	RT99, BA03
28978 Ixion	3.84 ± 0.03	0.138 ± 0.03	41	3.25 ± 0.04	0.144 ± 0.04	3	0.05	Bo04, All16
58534 Logos	7.41 ± 0.10	0.055 ± 0.08	5	6.72 ± 0.10	0.052 ± 0.09	4	0.14	All16
136472 Makemake	0.00 ± 0.01	0.206 ± 0.01	53	0.56 ± 0.07	-1.155 ± 0.09	6	0.03	All16
52872 Okyrhoe	11.40 ± 0.05	-0.013 ± 0.01	7	10.83 ± 0.05	0.020 ± 0.01	12	0.07	BA03, All16, TW
90482 Orcus	2.27 ± 0.02	0.159 ± 0.02	30	1.87 ± 0.03	0.216 ± 0.04	4	0.04	All16
49036 Pelion	10.89 ± 0.08	-0.064 ± 0.04	5	10.35 ± 0.07	-0.029 ± 0.04	6	0.14	BA03, All16
5145 Pholus	7.46 ± 0.31	0.152 ± 0.15	10	6.80 ± 0.29	0.111 ± 0.13	16	0.60	BA03, All16, TW

Table 4. Absolute Magnitudes

Object	H_V (mag)	β_V (mag per degree)	N_V	H_R (mag)	β_R (mag per degree)	N_R	Δm	Ref.
50000 Quaoar	2.77 ± 0.25	0.116 ± 0.22	45	2.19 ± 0.23	0.047 ± 0.24	8	0.30	Ba06,Al16
120347 Salacia	3.51 ± 0.06	0.665 ± 0.04	9	3.89 ± 0.03	-0.153 ± 0.04	10	0.03	Al16, TW
90377 Sedna	1.56 ± 0.01	0.640 ± 0.04	9	1.04 ± 0.00	0.166 ± 0.00	157	0.02	Ra07,Pe10,Al16
79360 Sila-Nunam	5.57 ± 0.22	0.095 ± 0.20	6	4.91 ± 0.16	0.132 ± 0.20	5	0.22	SJ02,Al16
32532 Thereus	9.44 ± 0.12	0.063 ± 0.02	69	9.00 ± 0.30	0.055 ± 0.05	17	0.34	Je15,BA03,Al16
42355 Typhon	7.66 ± 0.02	0.128 ± 0.01	22	7.12 ± 0.11	0.138 ± 0.04	5	0.07	Al16
174567 Varda	3.97 ± 0.04	-0.441 ± 0.06	10	3.24 ± 0.04	-0.024 ± 0.06	10	0.06	Al16, TW
20000 Varuna	3.96 ± 0.23	0.103 ± 0.24	30	3.29 ± 0.21	0.171 ± 0.27	20	0.50	Hi05,Be06, Al16

Table 5. **TW** = This work, Al16 = Alvarez-Candal et al. (2016), Ba00 = Barucci et al. (2000), Bo01 = Boehnhardt et al. (2001), Bo02 = Boehnhardt et al. (2002), Bo04 = Boehnhardt et al. (2004), Ca06 = Carry et al. (2012), Ca12 = Carry et al. (2012), DM09 = Carraro et al. (2006), Do01 = Delsanti et al. (2001), Ga16 = Galiazzo et al. (2016), GH01 = Gil-Hutton et al. (2001), Hi05 = Hicks et al. (2005), Je15 = Jewitt et al. (2015), JL01 = Jewitt et al. (2001), Mu04 = Mueller et al. (2004), Px04 = Peixinho et al. (2004), Pe13 = Perna et al. (2013), Ra07 = Rabinowitz et al. (2007), Ro05 = Rousset et al. (2005), Se02 = Sekiguchi et al. (2002), SJ02 = Sheppard et al. (2002), Sn10 = Snodgrass et al. (2010), SS09 = Santos-Sanz et al. (2009), Th12 = Thirouin et al. (2012), TR03 = Tegler & Romanishin (2003).